Remote Sensing of Environment 143 (2014) 85–96

Contents lists available at ScienceDirect

Remote Sensing of Environment

journal homepage: www.elsevier.com/locate/rse

The New VIIRS 375 m active fire detection data product: Algorithm description and initial assessment

Wilfrid Schroeder [a,*], Patricia Oliva [a], Louis Giglio [a], Ivan A. Csiszar [b]

[a] Department of Geographical Sciences, University of Maryland, College Park, MD, United States
[b] NOAA/NESDIS Center for Satellite Applications and Research, College Park, MD, United States

ARTICLE INFO

Article history:
Received 14 October 2013
Received in revised form 16 December 2013
Accepted 17 December 2013
Available online xxxx

Keywords:
Active fire detection
S-NPP/VIIRS
MODIS

ABSTRACT

The first Visible Infrared Imaging Radiometer Suite (VIIRS) was launched in October 2011 aboard the Suomi-National Polar-orbiting Partnership (S-NPP) satellite. The VIIRS instrument carries two separate sets of multi-spectral channels providing full global coverage at both 375 m and 750 m nominal resolutions every 12 h or less depending on the latitude. In this study, we introduce a new VIIRS active fire detection algorithm, which is driven primarily by the 375 m middle and thermal infrared imagery data. The algorithm builds on the well-established MODIS *Fire and Thermal Anomalies* product using a contextual approach to detect both day and nighttime biomass burning and other thermal anomalies. Here we present the fire algorithm's design and implementation, including important information describing the input data characteristics and potential artifacts associated with pixel saturation and the South Atlantic Magnetic Anomaly, both found to affect the middle infrared channel data. Initial assessment using results derived from the global processing of the algorithm indicated small, although variable, commission errors (<1.2%) for nominal confidence fire pixels. We achieved improved performance using the 375 m active fire data compared to the VIIRS 750 m baseline fire product, resulting in a 3× and 25× factor increase in the absolute number of fire pixels detected using day and nighttime data, respectively. Similarly, VIIRS 375 m fire data showed significantly superior mapping capabilities compared to current MODIS fire detection data with improved consistency of fire perimeter delineation for biomass burning lasting multiple days.

1. Introduction

The Visible Infrared Imaging Radiometer Suite (VIIRS) was launched in October 2011 aboard the Suomi National Polar-orbiting Partnership (S-NPP) satellite, a United States mission jointly managed by the National Aeronautics and Space Administration (NASA) and the National Oceanic and Atmospheric Administration (NOAA). The S-NPP serves as a preparatory mission to the upcoming Joint Polar Satellite System (JPSS), while delivering operational data products (Hillger et al., 2013). The JPPS program will provide continuity to the multi-decadal polar orbit environmental satellite data record that includes NOAA's Advanced Very High Resolution Radiometer (AVHRR) and NASA's Moderate Resolution Imaging Spectroradiometer (MODIS) data, and is complemented by data from the Defense Meteorological Satellite Program (DMSP) (Justice et al., 2013). These different satellite data sets have been used in support of a variety of active fire and biomass burning products and applications (Davies, Ilavajhala, Wong, & Justice, 2009; Elvidge et al., 1996; Flasse & Ceccato, 1996; Giglio, Descloitres, Justice, & Kaufman, 2003; Giglio, Loboda, Roy, Quayle, & Justice, 2009; Ichoku, Giglio, Wooster, & Remer, 2008; Roy, Boschetti, Justice, & Ju, 2008). The resulting fire products have reached different levels of maturity based on validation analyses and algorithm refinements made over the years, with the MODIS *Fire and Thermal Anomalies* algorithm (MOD14 and MYD14) becoming the most developed and widely used fire data set in the last decade (Giglio et al., 2003; Morisette, Giglio, Csiszar, & Justice, 2005; Schroeder et al., 2008).

The operational land products derived from the new VIIRS data include key Environmental Data Records (EDRs), and the Active Fires Application Related Product (ARP) in support of primarily weather applications (Justice et al., 2013). Originally, the VIIRS Active Fires ARP built on the 750 m channel data containing sparse array output data including the geographic (latitude and longitude) and image (row and column indices) coordinates, and associated quality flags describing fire-affected pixels (Csiszar et al., in press). The algorithm used to generate the current operational VIIRS 750 m Active Fires ARP builds on the MODIS Collection 4 fire algorithm (Giglio et al., 2003), applying virtually the same combination of tests to the corresponding VIIRS 750 m multi-spectral data. Subsequent revision of VIIRS land product requirements for the upcoming JPSS upgraded the 750 m Active Fires ARP product to the category of EDR. The revised requirements incorporated algorithm updates and additional layers to the product including a 2D image classification array (fire mask), a pixel-based fire characterization parameter (Fire Radiative Power [FRP]), among other features. The revised active fire product will be gradually integrated into the current

* Corresponding author at: Department of Geographical Sciences, University of Maryland, 2181 LeFrak Hall, College Park, MD 20742, United States. Tel.: +1 202 341 7763.
E-mail address: wilfrid.schroeder@noaa.gov (W. Schroeder).

0034-4257/$ – see front matter © 2014 Elsevier Inc. All rights reserved.
http://dx.doi.org/10.1016/j.rse.2013.12.008

S-NPP/VIIRS data processing stream thereby enabling full delivery of required data layers with the launch of the first JPSS satellite around 2017. In addition to the operational 750 m Active Fires ARP product, a new algorithm was recently developed using primarily the VIIRS 750 m short-wave infrared (1.61 μm) channel and Day-Night Band (DNB) data for the nighttime detection of gas flares and other high temperature sources (Elvidge, Zhizhin, Hsu, & Baugh, 2013).

Building on the current MODIS fire algorithm, the current operational VIIRS 750 m Active Fires ARP and future EDR active fire detection and characterization product will provide continuity to more than 10 years of systematic global biomass burning monitoring (Justice et al., 2002). Like MODIS, VIIRS 750 m Active Fires algorithm is primarily based on a dual gain high saturation temperature (634 K) middle infrared channel (4 μm) and on a single gain thermal infrared (11 μm) channel data, thereby accommodating a wide range of fire pixel radiances. Initial post-launch assessment of the VIIRS 750 m Active Fires ARP indicated good overall performance with high degree of agreement with near-coincident Aqua/MODIS active fire detections (Csiszar et al., in press). Compared to 1 km Aqua/MODIS MYD14 data, the VIIRS 750 m Active Fires ARP showed increased fire detection rates as a result of the radiometer's improved spatial resolution and unique sampling scheme. The sampling scheme applied to VIIRS data incorporates data aggregation processing to compensate for pixel footprint enlargement with distance from nadir (Cao, DeLuccia, Xiong, Wolfe, & Weng, 2013; Csiszar et al., in press).

In this study, we investigate the use of the complementary set of 375 m resolution VIIRS channels for active fire detection, in order to take full advantage of the finer spatial information provided by those data. Improved spatial resolution enables detection of smaller fires of the same temperature, as well as refined mapping of larger fires, resulting in critical gain to both fire management and science applications. The VIIRS five-channel 375 m data include two bands centered on the middle and thermal infrared regions. Consequently, it meets the basic spectral requirements for application of fire detection algorithms based on the differential radiometric response of high temperature targets imaged in those two spectral regions. We present the main data characteristics and describe the design and implementation of the active fire detection algorithm, and how it compares against the operational 750 m Active Fires ARP baseline fire product and other active fire data sets.

2. Input data characteristics

The S-NPP/VIIRS flies in a sun-synchronous orbit with an equator crossing local time of ~1:30 PM (ascending node) and ~1:30 AM (descending node), acquiring simultaneous and co-registered 375 m (I-bands) and 750 m (M-bands) resolution data. The VIIRS 375 m data are comprised of five distinct single-gain channels extending from the visible to thermal infrared spectral region (Fig. 1; VIIRS spectral response functions available at: http://www.star.nesdis.noaa.gov/jpss/VIIRS.php). The pixel size increase with scan angle, typical to other sensors such as AVHRR and MODIS, is minimized due to a unique data aggregation scheme performed for all VIIRS channels (Wolfe et al., 2013). This scheme results in three distinct image sections in the across track direction (Fig. 1). The native I-band image resolution prior to onboard aggregation is approximately 125 × 375 m at nadir. In the first image section (scan angles from 0° (nadir) to ±31.72°), every three native pixels are averaged over the radiance domain in the across track direction to form one effective sample. In the second image section (scan angles from ±31.72° to ±44.86°), every two native pixels are aggregated into one effective sample. Finally, no aggregation is performed in the third image section (scan angles from ±44.86° to ±56.28°) such that each native pixel represents one effective sample. Consequently, the first, second and third image sections total 1184, 736, and 1280 samples, respectively, and the effective footprint ranges from the nominal 375 m resolution (383 × 360 m) at the sub-satellite point to 795 × 784 m at a maximum scan angle of 56.28°. The image swath extends to approximately 3000 km, or 6400 pixels, providing complete global coverage every ≈12 h or less depending on the latitude.

Onboard pre-processing of VIIRS data is also applied to minimize data redundancy during scanning. Data redundancy results from the two-fold increase in sample footprint size from nadir to the edge of scan (also known as the *bowtie* effect), which is still observed after aggregation (Wolfe et al., 2013). An array of 32 detectors (compared to 16 on the 750 m channels) arranged along track generates 6400 × 32 samples during each rotation of the telescope. To minimize the bowtie effect, the four outermost sample rows of an individual scan (two on each end) are replaced with fill values across the second image section, whereas the eight outermost sample rows of an individual scan (four on each end) are replaced with fill values across the third image section. Deletion of those samples results in approximately 50% reduction in data redundancy in the Sensor Data Record (SDR). The bowtie deletion creates a striped pattern across the second and third image sections, which reflects the samples containing fill values (Fig. 2).

VIIRS channel I4 is the primary driver of the fire detection algorithm presented in this study. The spectral response of Channel I4 (ranging from 3.55 to 3.93 μm, centered at 3.74 μm) spans the wavelengths of peak spectral radiance for blackbodies emitting at temperatures between 737 and 817 K. Channel I4 is therefore well suited for distinguishing pixels containing sub-resolution combustion components from those pixels composed of cooler fire-free background areas. Channel I4 is a single gain channel with a pixel saturation

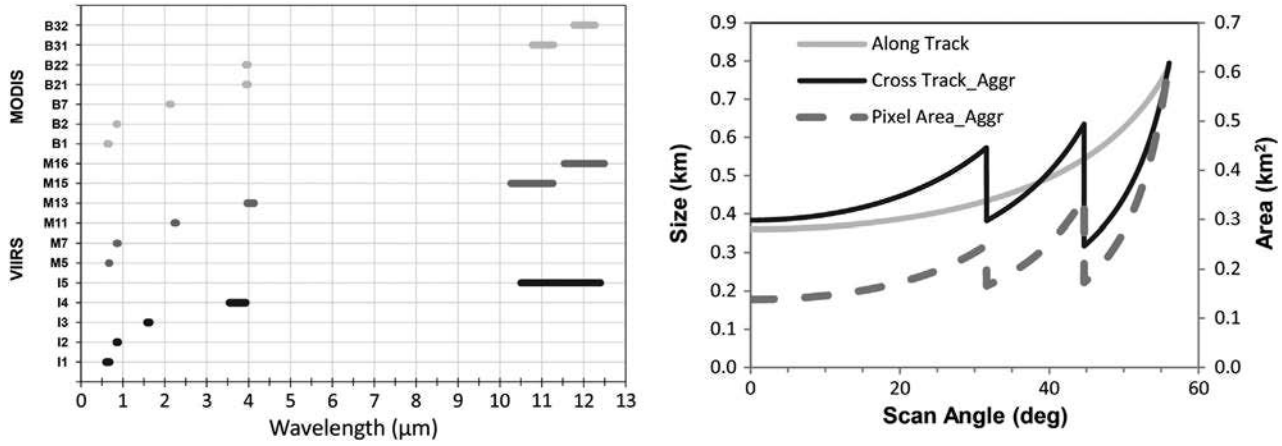

Fig. 1. VIIRS 375 m (I-bands) and 750 m (M-bands), and MODIS (B) data spectral intervals for all channels used in the corresponding active fire detection algorithms (left), and VIIRS I-band sample spatial resolution describing the along track, cross track (aggregated), and area (aggregated) dimensions (right).

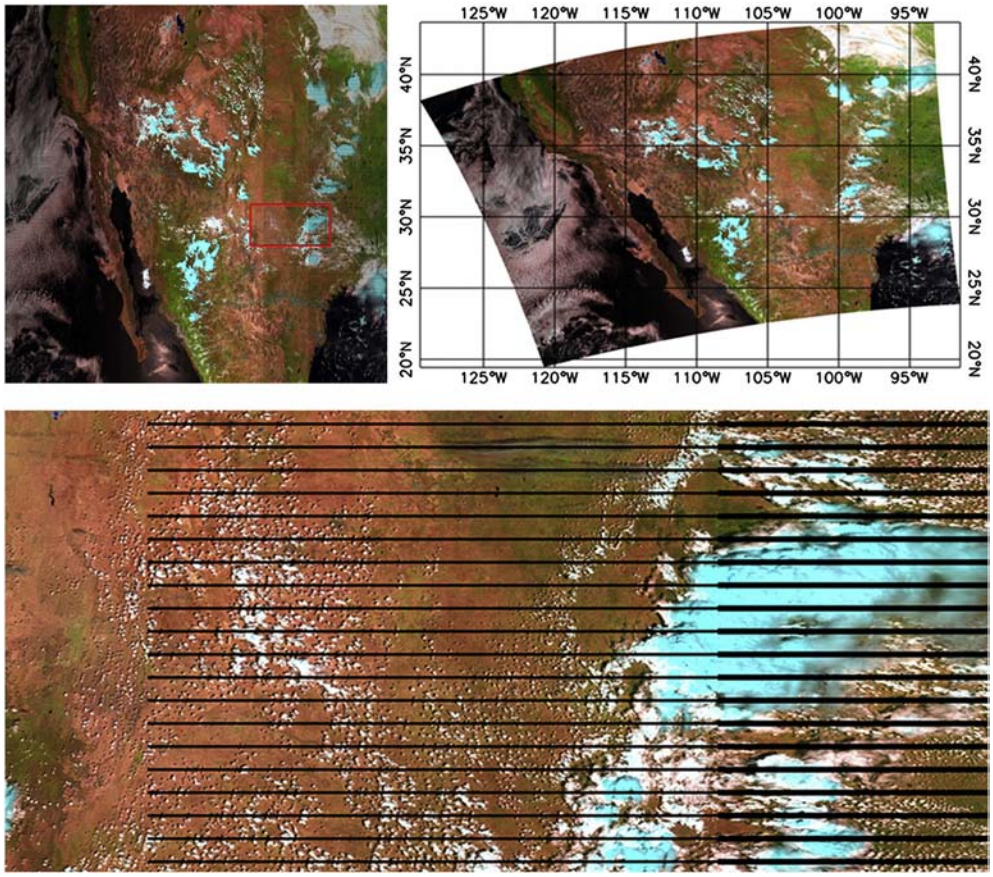

Fig. 2. VIIRS 375 m swath (satellite projection; top left) and resampled (geographic projection; top right) data acquired on 15 August 2013 20:16–20:21UTC over part of Mexico and United States. Lower panel comprises swath data subset (red rectangle) showing the striped pattern created by bowtie deletion (fill values) coincident with second and third image sections. (For interpretation of the references to color in this figure legend, the reader is referred to the web version of this article.)

temperature of 367 K. The relatively low saturation temperature, in combination with the improved spatial resolution, can result in frequent fire pixel saturation. This is therefore considered the most important channel characteristic influencing the development of an active fire algorithm for this data set, as will be demonstrated below. Another important aspect of VIIRS I4 data involves the channel's spectral placement, which is approximately 0.3 μm shorter than the corresponding VIIRS M13 radiometer channel driving the baseline 750 m Active Fires ARP algorithm. This spectral offset introduces an approximately three-fold increase of the reflected solar component in the I4 channel, with potential reduction of the radiometric separation between fire-affected pixels and bright fire-free surfaces.

Complementing the I4 channel data, channel I5 is centered at 10.5–12.4 μm and is the primary channel against which I4 is compared in order to separate active fires from their fire-free background. This is also a single gain channel with a saturation temperature of 380 K. The three remaining I-band channels (I1, I2, and I3) cover the visible (0.6–0.68 μm), near-infrared (0.846–0.885 μm) and the shortwave infrared (1.58–1.64 μm) regions and are used in support of cloud, sun glint and water-body discrimination in the fire detection algorithm. VIIRS channels I1–I3 are only operated during the daytime portion of the orbit.

The VIIRS SDRs used in this study were produced by the Interface Data Processing Segment (IDPS), and distributed as Hierarchical Data Format (HDF5) files corresponding to ~84 s orbit segments. Each SDR file contains 16-bit data from a single VIIRS channel. Geolocation data are distributed as a separate HDF5 file containing terrain-corrected pixel level navigation. Individual SDR files provide calibrated top-of-atmosphere (TOA) reflectance (unitless) and radiance ($W \cdot m^{-2} \cdot sr^{-1} \cdot \mu m^{-1}$) data for visible channels I1, I2, and I3, and scaled brightness temperature (K) and radiance data for infrared channels I4 and I5. Additional metadata complement the HDF5 file content, including pixel level 8-bit quality flags for each channel (JPSS, 2013). VIIRS SDRs include quality flags describing a range of calibration scenarios that can lead to anomalous pixel data and therefore are used to screen for such departures from nominal data quality. However, VIIRS SDR data lack detailed flagging or special handling of fire-affected and other radiometrically bright native pixels during the onboard data aggregation processing. This limitation can lead to potential artifacts in the data due to mixing of saturated and unsaturated pixels. A discussion of the implications to active fire detection is provided in Section 2.1 below.

2.1. Data artifacts

Assessment of the VIIRS data available to date (approximately two years of sensor operation at the time of writing) indicated two main anomalous conditions affecting the primary I4 channel used for active fire detection: pixel saturation and the South Atlantic Magnetic Anomaly (SAMA). Pixel saturation may be found over fires typically spreading over multiple contiguous pixels, an indication of potentially large and intense biomass burning (Fig. 3a–b). In the first instance, saturated pixels show a brightness temperature of 367 K and corresponding channel I4 SDR quality flag indicating "*poor calibration – all pixels saturated*". A second variation in pixel saturation is associated with very large wildfires where VIIRS pixels located at the core area coinciding with intense fire activity will greatly exceed the effective saturation temperature causing a complete folding of the digital count. In this case, the pixel's brightness temperature may be set at 208 K, the lower end of the channel I4 dynamic range (Fig. 3c). The corresponding SDR quality flag will predominantly associate the folding pixels with a "*poor*

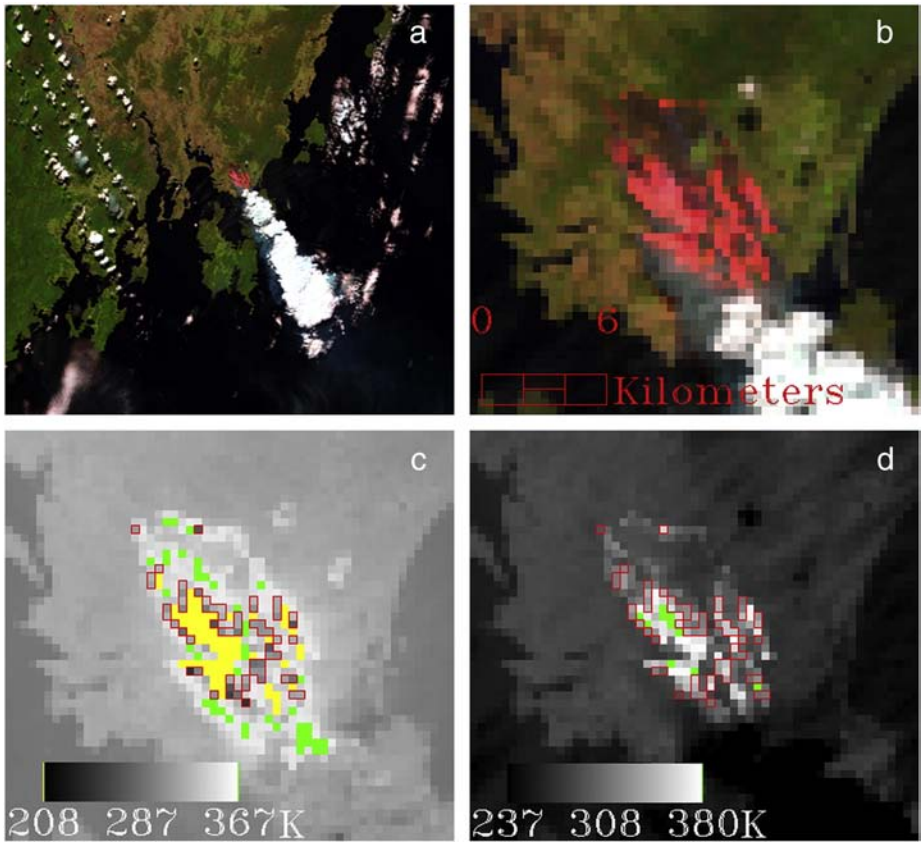

Fig. 3. (a) VIIRS 375 m visible RGB composite (channels 3-2-1) subset acquired at ~04:22UTC on 04 January 2013 over southern Tasmania/Australia showing a large active fire complex, which is zoomed in (b–d) to show details. (c) VIIRS I4 channel data showing folding of pixel digital count at the core of the main active fire fronts with a brightness temperature of 208 K (marked yellow), along with pixels of nominal saturation at a brightness temperature of 367 K (marked green). (d) VIIRS I5 channel data showing fewer saturated pixels with a brightness temperature of 380 K (marked green). Spurious (cooler) VIIRS I4 brightness temperature pixel values resulting from the potential mixing of saturated and unsaturated pixels during aggregation are outlined by the red vectors in (c); those pixels coincide with nominal quality high brightness temperature I5 channel as shown in (d). (For interpretation of the references to color in this figure legend, the reader is referred to the web version of this article.)

calibration – radiance out of range" condition, although occasional "*all pixels saturated*" flagging may occur. The third variation in pixel saturation involves the generation of artificially low brightness temperature values suggesting that saturated (including potential pixel data folding) and unsaturated native pixels are mixed together during aggregation (Fig. 3c). Mixed pixels are currently flagged as "*good quality*" in the SDR quality flag. In all cases involving the three scenarios above, I4 channel saturation may be determined by examination of the companion I5 channel brightness temperature data, which will typically show a higher absolute value compared to I4 (contrary to unsaturated fire-affected pixels which will always show higher brightness temperature values on the I4 channel compared to I5) (Fig. 3d).

The second anomalous condition affecting the I4 channel involves the occurrence of spurious brightness temperature data as a result of the SAMA. The geographic area where the problem is most commonly found extends from 110°W <> 11°E and 7°N <> 55°S (see for example Fig. 5, Section 4.2) (Cabrera et al., 2005; Casadio, Arino, & Serpe, 2012). The impact of the SAMA is evidenced by artificially high brightness temperature values in the nighttime I4 channel data. These occurrences are typically associated with nominal data quality and therefore cannot be readily identified nor excluded using the available quality flags. On average, individual I4 pixels affected by the SAMA may depart from the background by 15–30 K, thereby creating similar radiometric response associated with actual nighttime fire-affected pixels at both absolute and contextual levels. No discernable impact on nighttime I5 channel data quality was found associated with the SAMA.

3. Algorithm description

The active fire detection algorithm proposed here for the VIIRS 375 m resolution data builds on the MODIS *Fire and Thermal Anomalies*, taking advantage of several years of algorithm development, validation and refinement (Giglio et al., 2003; Kaufman et al., 1998; Morisette et al., 2005; Schroeder et al., 2008). While the most basic algorithm data input requirements are met with the available VIIRS I4 and I5 middle and thermal infrared and I1 and I2 visible channels, important differences in spatial resolution, sampling and spectral characteristics demand a new customized approach in order to optimize algorithm performance. Most notably, the reduced pixel saturation temperature of 367 K in the primary I4 fire detection channel, in combination with the channel's shorter wavelength compared to MODIS channels 21 and 22 (3.929–3.989 μm) and VIIRS M13 channel (3.973–4.128 μm), prevented direct application of the original MODIS detection tests as problems involving incorrect pixel classification quickly developed. In order to improve on that, first data dependencies were identified (namely by isolating pixel saturation scenarios and SAMA-related artifacts), and detection tests were then tuned to match the spatial and spectral characteristics of the data. Tuning was performed using several images acquired over different geographic regions and was based on histogram analyses of individual test results complemented by error matrix analysis. Initial test sample error assessment was based on visual inspection of the output fire detection data using expert analysis supported by higher resolution reference images from Google Earth and Landsat-8. The algorithm is customized for both day and night data

analyses, with the latter representing those pixels with a solar zenith angle ≥90°.

3.1. Initial data screening

3.1.1. Classification of cloud and water pixels

Pixels containing optically thick clouds are classified independently as part of the fire algorithm processing following the similar approach used in the heritage International Geosphere-Biosphere Programme (IGBP) and MODIS fire products (Giglio et al., 2003; Stroppiana, Pinnock, & Grégoire, 2000), on which the VIIRS 750 m Active Fires ARP product also builds upon. For daytime data, cloud pixels are classified using the following tests:

$BT_5 < 265$ K
OR
$\rho_1 + \rho_2 > 0.9$ AND $BT_5 < 295$ K
OR
$\rho_1 + \rho_2 > 0.7$ AND $BT_5 < 285$ K

where ρ_i is the reflectance in I-band channel i and BT_i is the brightness temperature in I-band channel i. For nighttime data, cloud pixels are classified based on the brightness temperature of channels I4 and I5 as follows:

$BT_5 < 265$ K AND $BT_4 < 295$ K.

Adding BT_4 to the nighttime cloud test improved algorithm response to fires occurring under semi-transparent clouds (e.g., cirrus), which can have very cold brightness temperatures on channel I5. The fire algorithm skips all day and nighttime pixels classified as cloud-covered, and their data are excluded from the calculation of fire pixel background conditions.

Water bodies were classified for daytime data using a spectral profiling approach using the following VIIRS I-band channel combination:

$\rho_1 > \rho_2 > \rho_3$.

This test can successfully separate most water bodies, whereas it tends to underperform over sediment-filled water pixels and along some shorelines. Also, burn scars may also be misclassified as water using the test above although this limitation had no observable impact on the active fire detection performance. The fire algorithm processes all pixels classified as water to allow for gas flare detection, although their data are excluded from the calculation of daytime background conditions.

3.1.2. Fixed threshold tests

Detection of unambiguous daytime fire-affected pixels based on a simple fixed threshold applied to VIIRS channel I4 brightness temperature data is not practical due to the spectral characteristics of that channel, which could lead to numerous potential false alarms. For nighttime data any potential ambiguity is eliminated and the following test was adopted:

$BT_4 > 320$ K AND $QF_4 = 0$ [nighttime only]

where QF_4 is the channel I4 quality flag, which must show nominal data quality.

Potential daytime and nighttime fire-affected pixels may be identified through the screening of channel I4 saturated pixels in combination with complementary data from channels I1, I2, and I5 applied to the following tests:

$BT_4 = 367$ K AND $QF_4 = 9$ [both day and night]

AND

BT_5 N290 K AND $QF_5 = 0$ [daytime only] AND $\rho_1 + \rho_2$b0.7 [daytime only]

where QF_i is the quality flag on channel i. In this case, the channel I4 quality flag (decimal) value indicates complete saturation of the aggregated pixel value and is found concurrently with channel I5 nominal quality data. This condition coincides with the first saturation scenario described above when channel I4 brightness temperature is set at the saturation value of 367 K. In order to address the saturation scenario when folding of the channel I4 data is encountered, a fire pixel detection test is implemented using:

$\{\Delta BT_{45} < 0$ [both day and night]

AND

($BT_5 > 325$ K AND $QF_5 = 0$ [daytime] OR
$BT_5 > 310$ K AND $QF_5 = 0$ [nighttime])}
OR
$\{BT_4 = 208$ K AND $BT_5 > 335$ K [nighttime]$\}$

where ΔBT_{45} is the channel I4 and I5 brightness temperature difference. Here, the negative difference between those two channels is indicative of artificially cold brightness temperature on channel I4 caused by complete folding of the aggregated pixel value, or mixing of folded and non-folded pixels during onboard aggregation. Typically, this condition is only observed at the core areas of large and very intense wildfires that are assumed to greatly exceed the effective I4 channel saturation temperature.

All fire pixels identified using the simple thresholding tests above are exempted from the contextual fire detection analysis (Section 3.3), thereby reducing the overall image processing time. However, daytime fire pixels undergo additional false alarm screening described in Section 3.4, whereas night pixels occurring in the SAMA region undergo additional verification described in Section 3.5.

3.1.3. Masking of potential background fires

Potential background fire pixels are identified using daytime and nighttime-specific tests as follows:

$BT_4 > 335$ K AND $\Delta BT_{45} > 30$ K [daytime only]
OR
$BT_4 > 300$ K AND $\Delta BT_{45} > 10$ K [nighttime only]

Potential background fire pixels are used below to supplement the characterization of background conditions for candidate fire pixels.

3.1.4. Avoiding bright fire-free targets

Radiometrically bright targets such as sand banks along riverbeds can form small clusters of high BT4 pixel values on daytime VIIRS I-band data, some of which may be confused with active fires. In order to avoid these areas, daytime pixels meeting the following criteria are automatically skipped:

$\rho_1 + \rho_2 > 0.6$ AND $BT_5 < 285$ K
AND
$\rho_3 > 0.3$ AND $\rho_3 > \rho_2$ AND $\rho_2 > 0.25$ AND $BT_4 \leq 335$ K.

3.2. Candidate fire pixels

Candidate pixels are defined using a less strict set of conditions to include potential background fire pixels plus other less prominent radiometric anomalies on channel I4. The candidate pixels are those meeting the following criteria:

$BT_4 > BT_{4s}$ OR $\Delta BT_{45} > 25$ K [daytime only]
OR
$BT_4 > 295$ K OR $\Delta BT_{45} > 10$ K [nighttime only]

where BT_{4s} is a large-area background brightness temperature reference value on channel I4 calculated for a 501 × 501 window centered on the

pixel. This initial large-area sampling accommodates variations in background conditions, adding flexibility to candidate fire pixel selection. It is intended to improve algorithm sensitivity to fires occurring in colder high latitude regions, while reducing false alarm rates in lower latitudes consisting of warmer background. The large area background sampling excludes all pixels previously classified as cloud, water bodies, and potential background fire pixels, as well as any pixel with non-zero quality flag including fill values associated with bowtie deletion samples. BT_{4s} is derived using the following:

$$BT_{4M} = Max[325, M]\ \mathrm{K}$$
$$BT_{4s} = Min[330, BT_{4M}]\ \mathrm{K}$$

where M is the BT_4 median value calculated for the 501 × 501 window. The sampling window must contain a minimum of 10 valid observations or else BT_{4s} is set to 330 K. BT_{4s} is only derived for daytime data, allowing the candidate fire pixel brightness temperature on channel I4 to vary between a minimum of 325 K to a maximum of 330 K in order to accommodate scene-dependent changes in background conditions. Nighttime background conditions are found to be less variable, therefore we opted to use a single fixed value to define candidate fire pixels at night.

3.3. Contextual analysis

The contextual analysis implemented for VIIRS 375 m fire detection resembles the MODIS *Fire Thermal Anomalies* algorithm approach by sampling a dynamically assigned window size to allow optimum characterization of the candidate fire pixel background. In the VIIRS I-band case, the minimum sample size is set to an 11 × 11 element window centered on the candidate fire pixel. The sampling window is allowed to grow to a maximum size of 31 × 31 until at least 25% of the sample size is composed of valid pixels, or a minimum of 10 valid pixels are found. Similarly to the large area background sampling applied to the daytime data, valid pixels exclude those classified as cloud, water bodies, potential background fire pixels, and pixels with non-zero quality flags on any of the input bands, including those containing fill values. If the minimum number of valid pixels cannot be met, the pixel is assigned the class "*unknown*" indicating that the background condition could not be properly characterized.

Provided the minimum number of background valid pixels is satisfied, mean and mean absolute deviation values are calculated for channels I4 $(\overline{BT}_{4b}, \bar{\delta}_{4b})$, I5 $(\overline{BT}_{5b}, \bar{\delta}_{5b})$, and the I4–I5 brightness temperature difference $\overline{BT}_{45b}, \delta_{45b}$ using the background sample. In addition, mean and mean absolute deviation are calculated for channel I4 brightness temperature data from potential background fire pixels found within the sampling window $\left(\overline{BT}_4', \bar{\delta}_4'\right)$. The parameters above are used to define a set of contextual tests that must be jointly satisfied in order to produce a nominal confidence fire pixel detection based on the criteria below:

Daytime :
$\Delta BT_{45} > \Delta\overline{BT}_{45b} + 2 \times \delta_{45b}$
$\Delta BT_{45} > \Delta\overline{BT}_{45b} + 10$
$BT_4 > \overline{BT}_{4b} + 3.5 \times \delta_{4b}$
$BT_5 > \overline{BT}_{5b} + \delta_{5b} - 4\ OR\ \delta_4' > 5$

Nighttime :
$\Delta BT_{45} > \Delta\overline{BT}_{45b} + 3 \times \delta_{45b}$
$\Delta BT_{45} > \Delta\overline{BT}_{45b} + 9$
$BT_4 > \overline{BT}_{4b} + 3 \times \delta_{4b}$.

The tests above explore the distinct radiometric signature associated with active fires, which will typically produce a strong departure of the fire-affected pixel brightness temperature on VIIRS channel I4 compared to fire-free adjacent pixels. The I4 channel response is accompanied by a relatively small variation on VIIRS channel I5 brightness temperature values relative to the same background. Test configuration is meant to avoid other image features with high channel I4 brightness temperatures such as clouds, and bright and warm surfaces such as deserts.

A complementary contextual test is applied to daytime data when the number of potential background fire pixels exceeds 10% of all valid background pixels in the sampling window, and is also greater than four pixels. This additional test is represented as follows:

$$\rho_2 > 0.15\ AND\ \overline{BT}_4' < 345\ AND\ \delta_4' < 3\ AND\ BT_4 > \overline{BT}_4' + 6 \times \delta_4'[\text{daytime only}].$$

This test targets desert boundary areas where the mixing of high and low temperature land surfaces could lead to erroneous pixel classification. All candidate fire pixels meeting the test above are automatically rejected.

3.4. Daytime false alarm filter

Sources of potential confusion found on the daytime VIIRS I-band data are treated independently using custom filters to reduce false alarm rates. Areas of high solar reflection are the primary cause of false alarms resulting in localized spikes in brightness temperature on channel I4 off metallic rooftops in industrial parks, over large and bright surfaces such as concrete pavement, and at water bodies over which specular reflection (Sun glint) may occur. In order to address this condition, a test is applied to all daytime nominal confidence fire pixels detected with the tests above using the angle θ_g between vectors pointing in the surface-to-satellite and specular reflection directions as in Giglio et al. (2003):

$$\cos\theta_g = \cos\theta_v \cos\theta_s - \sin\theta_v \sin\theta_s \cos\phi$$

where θ_g and θ_s are the view and solar zenith angles, respectively, and ϕ is the relative azimuth angle. Using the expression above, pixels classified as fire-affected by the previous tests are further inspected and downgraded to the class of "*glint-related false alarm*" if they satisfy the following condition:

$$\theta_g < 15^\circ\ AND\ \rho_1 + \rho_2 > 0.35$$
$$OR$$
$$\theta_g < 25^\circ\ AND\ \rho_1 + \rho_2 > 0.4.$$

In addition to the test above, a 3 × 3 ring is used around all remaining pixels classified as fire for which $\Delta BT_{45} < 30K$ *or* $\theta_g < 15°$ to look for low confidence detections. Single stand-alone fire pixels (i.e., those without adjacent detections) with a channel I4 brightness temperature less than 15 K above any of the valid adjacent eight pixels forming the ring are assigned a "*low confidence*" class; valid pixels are defined as in the background sampling methods described above. If no valid pixels are found, the pixel is also assigned a "*low confidence*" class.

3.5. Nighttime SAMA filter

The influence of the SAMA on channel I4, as described in Section 2.1, can lead to numerous false alarms in the VIIRS nighttime data as the vast majority of pixels affected will mimic the radiometric signature of active fires. In order to minimize the negative impact of that anomalous feature on the output product, a filter based on the complementary VIIRS M13 channel data is used to further inspect pixels classified as nominal confidence fire detections by the nighttime tests and occurring within the region of influence of the SAMA. The application of this additional filter is restricted to stand-alone night fire pixels, as inspection of the first two years of VIIRS data indicated that manifestation of the

SAMA on the I4 channel is typically associated with single pixel events scattered over large regions.

First, the M13 brightness temperature [*x*, *y*] image coordinate is derived from the corresponding 375 m fire pixel. Then, a simple neighboring analysis is performed using a 3 × 3 ring centered on that location comparing the M13 brightness temperature of the target pixel with all adjacent pixels. The 375 m fire pixel is downgraded to a "*low confidence*" class if the M13 brightness temperature of the target pixel is found to be less than 1 K above all adjacent pixels. Otherwise, provided the coincident M13 brightness temperature is also indicative of a heat anomaly, the pixel is confirmed as a nominal confidence fire detection.

4. Results

4.1. Theoretical minimum detectable fire

We assessed the theoretical performance of the fire detection algorithm by simulating different fire scenarios applied to actual VIIRS 375 m global imagery. Fires were simulated assuming areas ranging from 2 to 250 m^2, and temperatures ranging from 400 to 1200 K. Fire radiances were derived at 2 m^2 and 10 K intervals for both I4 and I5 channels using the instrument's spectral response functions, and assuming blackbody emission. A total of 10 daytime and 10 nighttime VIIRS 5-min orbit segments acquired during August 2013 were randomly selected covering different geographic areas, including low and high latitude regions, with variable levels of fire activity. For every image, we selected 10 pixels distributed along nadir and apart from each other, and when possible, near areas of fire activity in order to best represent regional fire-prone conditions. Simulated fire radiances and actual background radiances were area-weighted to provide realistic BT4 and BT5 pixel values representative of actual observation conditions. The new VIIRS 375 m active fire detection algorithm was then applied to the imagery data containing a simulated active fire pixel surrounded by genuinely observed background pixels.

Fig. 4 shows the 50% probability of detection curves derived for the daytime and nighttime fire algorithms applied to the global data sample. Improved nighttime performance resulted from the more homogeneous background conditions, significantly enhancing the algorithm's response to relatively small heat sources. An experimental fire consisting of a 1.25 m radius circular bonfire burning at ~1000 K corroborated the night fire detection curve. The burn was conducted on 08 July 2013 near Rio de Janeiro, Brazil (43°00′00″W 22°23′36.6″S), coincident with the VIIRS overpass at 1:23 am local time. The fire was imaged by VIIRS at a 32.7° scan angle producing a +10 K increment over the I4 channel background, consequently satisfying all contextual tests in the nighttime fire algorithm. Meanwhile, daytime algorithm performance is subjected to the solar component, which introduces larger background variations and potential ambiguity involving highly reflective fire-free surfaces on channel I4. Consequently, the simulated daytime probability of detection was found to be lower compared to the same heat sources introduced in the nighttime data.

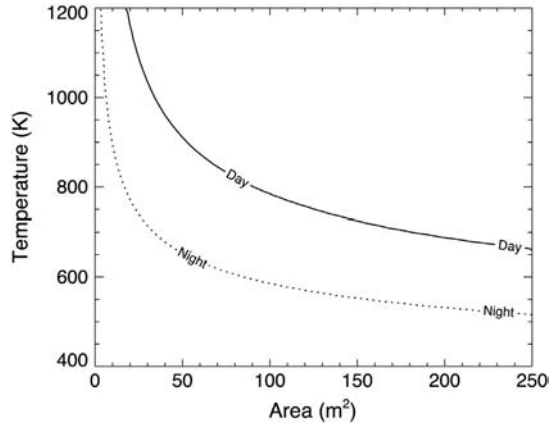

Fig. 4. Theoretical 50% probability of fire detection curves derived for VIIRS 375 m day and nighttime algorithms as a function of fire area and temperature.

Despite the differences between day and nighttime algorithm theoretical fire detection probability curves indicated here, actual product performance suggests that diurnal variations in fire behavior could help reduce that contrast. For example, larger and/or more intense biomass burning, typical of VIIRS early afternoon overpass times when dryer and warmer fuel and weather conditions prevail (Beck, Alexander, Harvey, & Beaver, 2002; Smith et al., 2013), should favor separation of active fire pixels from background. Conversely, smaller and/or cooler night fires could partially offset the improved separation of fire-affected pixels from a background with no solar component. Consequently, we expect this to lead to more uniform detection rates for same size fires burning during day and night observations (see for example Figs. 8 and 9, Sections 4.2.1 and 4.2.2).

4.2. Global fire detection performance

The performance of the 375 m active fire detection algorithm is demonstrated here for 30 days of global VIIRS data covering 1–30 August 2013. The algorithm was applied to both day and nighttime data, and the results compared to VIIRS 750 m Active Fires ARP (IDPS version) and Aqua/MODIS 1 km (MYD14) active fire detection products.

Fig. 5 shows the spatial distribution of daytime and nighttime fire detections produced by the VIIRS 375 m fire algorithm, plus low confidence daytime pixels potentially associated with bright fire-free land surface features and low confidence nighttime pixels identified across the SAMA region. On average, ~59,000 daytime and ~15,000 nighttime nominal confidence fire pixels were detected daily during the period sampled.

The application of the special filter to separate lower confidence nighttime pixels was effective in eliminating the vast majority of detections induced by the SAMA. However, on average 3 nighttime pixels of nominal confidence were detected daily over suspicious locations (e.g., pixels over open ocean away from known heat sources). Lack of appropriate reference data prevented further inspection of those isolated pixels; these cases represented 1% of all low confidence nighttime pixels detected over ocean in the SAMA region. Application of the nighttime false alarm filter across the SAMA region was also found to produce occasional omission errors for small and low intensity fires without a measurable heat signature on channel M13. Examples of confirmed omission errors induced by the SAMA filter were observed over known inland gas flares. Overall, commission and omission errors across the SAMA region were found to be reduced based on visual image inspection; further investigation using quality reference data is required in order to quantitatively estimate those potential errors. The number of low confidence fire pixels in the SAMA region accounted for approximately 5% of all nighttime fire pixels detected globally.

Daytime commission errors were typically found over bright land surfaces in areas of Sun glint. Those pixels were predominantly associated with reflective rooftops on large industrial buildings. Commission error rates were estimated for the nominal confidence daytime fire pixels by sampling single orbit data subsets distributed over 12 distinct 10° × 10° regions around the globe (Fig. 6). The data sample covered a wide range of land surface conditions, including areas with different fire regimes and subject to different levels of urban development. Areas in eastern China were particularly prone to produce false alarms showing a 1.2% commission error rate. Those cases were ambiguous to low confidence daytime pixels and were often observed over large industrial buildings containing highly reflective rooftops. In those areas the building materials and the landscape configuration, which is characterized by large industrial parks surrounded by cooler background, were found to augment the ambiguity between fire-free and fire-affected pixels. The daytime commission error rate for nominal confidence detections predominantly associated with urban false alarms was assessed using

Fig. 5. VIIRS 375 m fire algorithm output showing the accumulated daytime nominal confidence fire pixels (red; upper left), low confidence daytime pixels (light blue; upper right), nighttime fire pixels (purple; lower left), and SAMA-related low confidence nighttime pixels (dark blue; lower right) during 01–30 August 2013. (For interpretation of the references to color in this figure legend, the reader is referred to the web version of this article.)

visual analyses of pixel coordinates on Google Earth and estimated globally at 0.03%. Nighttime commission errors outside of the SAMA region were considered negligible based on visual inspection of VIIRS I-band channels, supported by higher resolution reference image from Google Earth. Nighttime detections were largely associated with elliptical-shaped pixel clusters typical of active fire fronts, spatially coincident with known heat sources (e.g., active volcanoes, gas flares, iron mills), or scattered around active biomass burning areas.

Daytime false alarm rates for low confidence pixels were estimated using the same global sample based on 12 different regions described above. On average 6% of low confidence daytime pixels were linked to urban environment and bright rooftops extending over a full pixel. Confirmed false alarms associated with low confidence daytime pixels peaked over eastern China at a rate of nearly 40%. Visual inspection of those locations using higher resolution images such as provided by Google Earth showed no indication of thermal heat sources; we therefore attributed the occurrence of those pixels to high solar reflection resulting in enhanced I4 channel brightness temperatures. Other areas with large absolute numbers of low confidence daytime pixels such as southern Africa showed predominant occurrence of those pixels along

Fig. 6. Regional subsets used for the estimation of VIIRS 375 m active fire algorithm commission errors. Boxes describe the date and time of the data subset used for each region, the number of detections sampled, and the confirmed false alarm rate.

the edge of fire pixel clusters of nominal confidence; therefore we associated those cases with lower intensity sub-pixel fire activity. Daytime low confidence fire pixels accounted for approximately 11% of all daytime detections produced globally.

Nominal saturation on channel I4 impacted approximately 8% of all daytime fire pixels detected, compared to 0.02% on channel I5. Nighttime saturation rates were equivalent to 1% on channel I4 and negligible on channel I5. Folding of the I4 digital value occurred for 0.2% of the fire pixels detected, whereas no pixel folding was identified on channel I5. Additionally, suspicious brightness temperature values on channel I4 were found for 0.5% of the daytime and 0.04% of the nighttime fire pixels in association with potential mixing of saturated and unsaturated native pixel radiances during onboard data aggregation. As described above, nominal pixel saturation and folding episodes were all accompanied by SDR flags indicating poor data quality. Meanwhile, the suspicious brightness temperature values involving potential mixing of saturated and unsaturated pixels were all accompanied by nominal SDR quality data flags. Due to the non-negligible rate of pixel saturation on channel I4 and the potential idiosyncrasies involving the SDR quality flags, we opted to defer the retrieval of sub-pixel fire characteristics such as FRP, size and temperature to future studies pending proper investigation of the complementary use of the dual-gain M13 channel data in support of those analyses.

4.2.1. Comparison with VIIRS 750 m Active Fires ARP

The VIIRS 375 m active fire detection data were compared to the operational VIIRS 750 m Active Fires ARP detection data generated by IDPS in order to assess the overall consistency between products. VIIRS 375 m and 750 m data are acquired simultaneously, and spatially co-registered (one 750 m pixel overlaps with four [2 × 2] 375 m pixels). Day and nighttime results were analyzed separately, as both algorithm and observation conditions differ in each case. Overall, VIIRS 375 m fire algorithm showed a three-fold increase in the absolute number of daytime fire pixels detected compared to the 750 m Active Fires ARP product, and a staggering 25-fold increase in the absolute number of nighttime fire pixels detected compared to the 750 m fire product. The number of coincident daytime detections produced by both data sets (i.e., one 750 m Active Fires ARP fire pixel with a minimum of one and a maximum of four overlapping 375 m nominal confidence fire pixel; Fig. 7a–b, dashed lines) accounted for 43% and 83% of the 375 m and 750 m fire pixels, respectively. Further consideration of 375 m low confidence daytime fire pixels helped increase the rate of coincident detections to 90% of the 750 m fire pixels. Meanwhile, the number of coincident nighttime detections accounted for 10% and 98% of the 375 m and 750 m fire pixels produced, respectively. These statistics reflect a significantly higher rate of fire detection using the 375 m data at night compared to the 750 m product (Fig. 7a–b; solid lines).

Differences in day and nighttime performance observed for the two VIIRS fire detection data sets also applied to spatially coincident clusters of contiguous fire pixels. Fig. 7c–d shows density plots of spatially coincident fire pixel clusters detected by the 375 m and 750 m fire algorithms, ranging in size from 1 to 10 contiguous pixels in each case. Coincident fire pixel clusters in the nighttime data were largely skewed towards the lower part of the plot area, indicating the occurrence of multiple contiguous 375 m fire pixels overlapping with smaller 750 m pixel clusters often containing less than two contiguous pixel elements.

Fig. 7. Frequency of VIIRS 375 m fire pixels with (dashed line) and without (solid line) coincident 750 m active fire detection for daytime (a) and nighttime (b) data during 1–30 August 2013. The horizontal axis indicates the number of VIIRS 375 m fire detections contained within each 750 m pixel footprint. Density plot showing the size of coincident fire pixel clusters detected using VIIRS 375 m and 750 m daytime (c) and nighttime (d) data.

Fig. 8. VIIRS 375 m and 750 m fire detection data acquired at 14:28 h PDT on 06 August 2013 and at 2:50 h PDT on 07 August 2013 over the Power Fire in California. USDA-Forest Service NIROPS airborne data acquired at 21:36 h PDT on 06 August 2013 shows the mapped fire perimeter as well as the areas showing intense heat.

The occurrence of lower intensity fires at night may help explain the results above, since those fires could fall below the detection limit of the 750 m product as suggested by the flat response of the 750 m product to smaller 375 m fire pixel clusters (Fig. 7b). Meanwhile, the occurrence of large 375 m fire pixel clusters with 1–2 750 m coincident pixels suggests potential omission errors in the IDPS product. The VIIRS 750 m Active Fires ARP product generated by IDPS is a replica of the Collection 4 MODIS *Fire and Thermal Anomalies* algorithm, modified to accept VIIRS data format. Consequently, tuning of the 750 m fire algorithm processed by IDPS to the VIIRS sensor-specific characteristics may be required.

The relative performance of the 375 m and 750 m fire detection algorithms was assessed using reference airborne fire data acquired by the U.S. Department of Agriculture – Forest Service National Infrared Operations (NIROPS) over wildfires in the United States in 2012 and 2013. Fig. 8 shows VIIRS 375 m and 750 m active fire detection clusters detected approximately 7 h before and 5 h after the NIROPS mapping of the Power Fire in California around 21:36 h PDT on 06 August 2013. The first VIIRS overpass represents the daytime data acquisition, whereas the second overpass coincides with the nighttime data approximately 12 h later. VIIRS 375 m detections are color-coded using the middle-infrared channel I4 brightness temperature data in order to provide a proxy for fire intensity across the complex at the moment of overpass. Differences between day and night data may be due to changes in fire behavior and background conditions as well as a result of the solar contribution in the middle-infrared channel. The daytime VIIRS fire detections derived from the 375 m and 750 m data showed good spatial agreement, and were well aligned with the underlying NIROPS fire perimeter and intense heat areas. The nighttime VIIRS 375 m data showed a small noticeable spatial progress of the 375 m fire cluster moving in the northeast direction, while maintaining good overall spatial agreement with NIROPS. The nighttime 750 m fire cluster was reduced to the northeastern part of the complex, omitting the cooler southwestern portion of the fire complex.

4.2.2. Comparison with MODIS

For more than a decade the *Fire and Thermal Anomalies* product has been among the most commonly used data set of the MODIS land product suite, serving both fire managers and the fire science community. The new VIIRS 750 m Active Fires EDR data will provide continuity to that invaluable data set into the next decade, delivering similar fire detection and characterization information to the user community. The VIIRS 375 m fire detection data complement the 750 m fire product, and could represent a significant improvement over the current MODIS 1 km data providing spatially refined fire information. To illustrate the potential qualitative gain in performance of the new VIIRS 375 m data compared to current MODIS 1 km product we analyzed a fire complex in southern Brazil. That fire burned for several days in March of 2013 and was imaged by VIIRS and MODIS onboard Terra and Aqua (Fig. 9). The fire data derived from sequential VIIRS 375 m images showed spatially consistent day and night fire detection clusters, and was estimated to spread at a rate of 58 m/h. Comparatively, the

Fig. 9. Daily fire spread mapped by 1 km Terra/MODIS (left), 375 m VIIRS (center), and 1 km Aqua/MODIS (right) data for a wildfire at the Taim Ecological Reserve in southern Brazil (−32.7°lat, −52.55°lon). The data cover the period beginning on 26 March 2013 (Julian day 85) and ending at the approximate time of the Landsat-7 data acquired at 13:15UTC on 31 March 2013. The white vector outline represents the burned area mapped using the 30 m Landsat-7 data.

MODIS 1 km fire detection data showed much less coherent fire spread information as a result of partial omission of the fire complex, as well as due to limited coverage provided by MODIS data at that latitude. Consequently, fire spread could not be properly estimated using MODIS data. Additionally, the VIIRS active fire pixels provide significantly improved spatial agreement with the available burned area perimeter digitized using Landsat-7 data acquired on 31 March 2013.

4.2.3. Comparison with Landsat-8

Previous satellite fire remote sensing validation studies used both coincident and near-coincident Advanced Spaceborne Thermal Emission and Reflection Radiometer (ASTER) and Landsat-5 and 7 data to quantify commission and omission errors for MODIS and Geostationary Operational Environmental Satellite (GOES) active fire products (Giglio et al., 2008; Morisette et al., 2005; Schroeder et al., 2008). In the case of VIIRS and Landsat-8 sensor data, the average 3 h separation between same-day image acquisition times prevents application of the paired data sets for quantitative error analyses, as artifacts associated with short-term variations in fire behavior can be introduced (Csiszar & Schroeder, 2008). However, Landsat-8 images may still be used as a reference data set in support of qualitative assessment of the VIIRS 375 m fire detection data allowing for visual interpretation of areas of active biomass burning.

Fig. 10 shows an active fire region in Melville Island/Australia imaged by Landsat-8 on 24 July and 09 August 2013. The VIIRS images for those two dates were acquired approximately 75 min after the Landsat-8 overpass. Areas showing active fire fronts could be separated on the Landsat-8 data using a fire detection algorithm based on the visible and shortwave infrared channels 5 and 7, similar to Schroeder et al. (2008). Burn scars can also be identified adjacent to the active fires. Visual analysis of the Landsat images shows the fire-affected area expanding outward in all directions, and particularly to the east and west of the large fire fronts detected on 24 July 2013. Overall, the instantaneous VIIRS 375 m fire detection data captured most of the near-

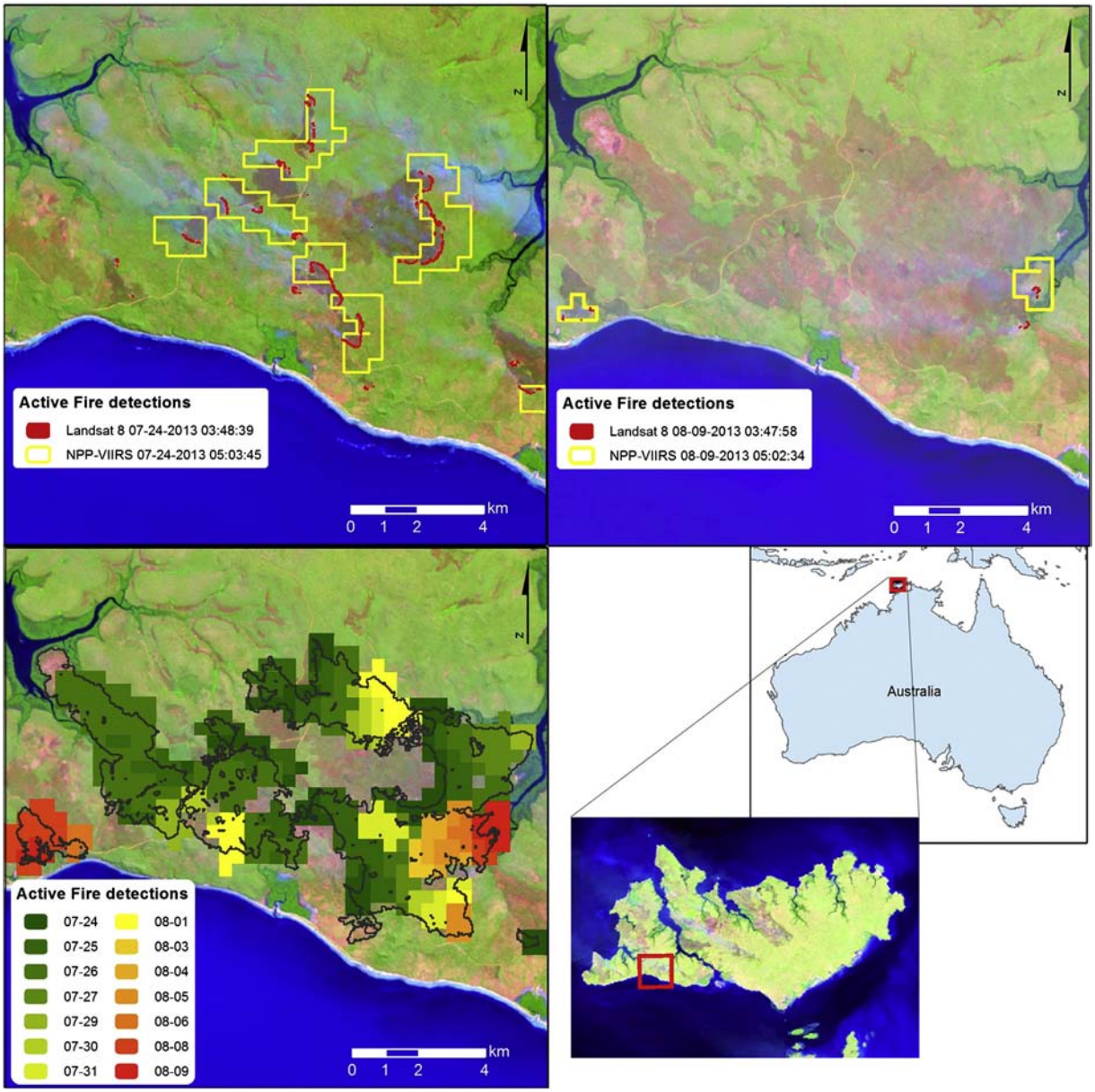

Fig. 10. Landsat-8 image subsets acquired on 24 July (upper left) and 09 August (upper right) 2013 over the Melville Island in Australia. Active fire fronts on Landsat-8 are marked red. Also shown are the VIIRS 375 m fire detection data (yellow vectors) acquired approximately 75 min after the Landsat-8 images. The lower left panel shows the accumulated VIIRS 375 m fire detection pixels during the time interval separating the two Landsat-8 acquisition dates, color-coded to indicate the calendar day of detection. The black vector shows the burned area perimeter mapped using dNBR applied to Landsat-8 data. (For interpretation of the references to color in this figure legend, the reader is referred to the web version of this article.)

coincident Landsat-8 active fire perimeter. Small differences could be identified and we assumed that those were caused by short-term variations in fire behavior, and due to differences in detection performance between the two data sets. The VIIRS fire detections accumulated over the period separating the acquisition dates of the two Landsat-8 scenes showed good spatial overlap with the 30 m resolution burned area mapped using differenced Normalized Burned Ratio (dNBR), providing further temporal information on the fire growth during that 16-day period.

5. Conclusions

In this paper we introduced the use of the new 375 m VIIRS sensor data in support of active fire detection using a contextual algorithm built on the heritage MODIS *Fire and Thermal Anomalies* product. Differences in VIIRS I-band spatial and spectral resolution were all addressed with the new algorithm. The new data set provides significantly refined spatial fire information, improving upon the current line of coarser spatial resolution satellite active fire detection products. The lower 367 K pixel saturation temperature in the middle-infrared I4 channel, combined with the pixel's smaller ground footprint, resulted in frequent saturation of fire-affected pixels. While the impact on active fire detection performance could be minimized, this condition created additional challenges to the retrieval of sub-pixel fire characterization parameters such as FRP, size and temperature. Alternatively, use of the 750 m dual-gain M13 channel data, which saturates at 634 K, could help complement the 375 m fire detection data providing unsaturated input data for the retrieval of sub-pixel fire characteristics; this is the subject of ongoing investigation.

The VIIRS improved spatial sampling, which eliminates coverage gaps over lower latitudes and minimizes pixel size increase with scan angle, provided consistent daily fire mapping performance of fires lasting several days. Our initial data quality assessment indicated high level of agreement between VIIRS 375 m fire detection data and near-coincident higher resolution airborne and Landsat-8 reference data sets. The classification of pixels into two main classes, namely nominal and low confidence groups, helped separate confirmed fire-affected pixels from ambiguous pixels more likely associated with false alarms and marginal burning.

The availability of spatially-refined active fire perimeter derived from 12 h VIIRS 375 m data provides new opportunities for using satellite fire information in support of fire tactical mapping and modeling applications. New applications building on these data have successfully demonstrated the assimilation of fire perimeter information derived from VIIRS 375 m fire data into higher resolution fire behavior models (Coen & Schroeder, 2013). Similar new applications are likely to follow.

Future development of the VIIRS 375 m algorithm described here shall explore the complementary use of the 750 m data, leading to a potential hybrid algorithm based on both sets of data. The current 375 m fire algorithm is intended for implementation as part of the International Polar Orbiter Processing Package (IPOPP) in order to serve the broader international community. Presently, routine data covering the Conterminous United States can be accessed at the following URL: http://viirsfire.geog.umd.edu/data.html.

Acknowledgments

This study was supported by the NASA Terrestrial Ecology and Applied Sciences Programs through the following research grants: NNX12AQ87G and NNH11AS03I. We are thankful for USDA's Remote Sensing Applications Center (Mr. Brad Quayle), National Infrared Operations (Mr. Thomas Mellin), and Pacific Southwest Research Station (Dr. Philip Riggan) for supporting initial data quality assessment in the United States.

References

Beck, J. A., Alexander, M. E., Harvey, S. D., & Beaver, A. K. (2002). Forecasting diurnal variations in fire intensity to enhance wildland firefighter safety. *International Journal of Wildland Fire*, *11*, 173–182.

Cabrera, J., Cyamukungu, M., Stauning, P., Leonov, A., Leleux, P., Lemaire, J., et al. (2005). Fluxes of energetic protons and electrons measured on board the Oersted satellite. *Annales Geophysicae*, *23*, 2,975–2,982.

Cao, C., DeLuccia, F., Xiong, X., Wolfe, R., & Weng, F. (2013). Early On-orbit Performance of the Visible Infrared Imaging Radiometer Suite (VIIRS) onboard the Suomi National Polar-orbiting Partnership (S-NPP) Satellite. *IEEE Transactions on Geoscience and Remote Sensing*. http://dx.doi.org/10.1109/TGRS.2013.2247768.

Casadio, S., Arino, O., & Serpe, D. (2012). Gas flaring monitoring from space using ATSR instrument series. *Remote Sensing of Environment*, *116*, 239–249.

Coen, J., & Schroeder, W. (2013). Use of spatially refined satellite remote sensing fire detection data to initialize and evaluate coupled weather-wildfire growth model simulations. *Geophysical Research Letters*. http://dx.doi.org/10.1002/2013GL057868.

Csiszar, I., & Schroeder, W. (2008). Short-term observations of the temporal development of active fires from consecutive same-day ETM+ and ASTER imagery in the Amazon: Implications for active fire product validation. *IEEE Journal of Selected Topics in Applied Earth Observations and Remote Sensing*, *1*(4), 248–253.

Csiszar, I., Schroeder, W., Giglio, L., Ellicott, E., Wind, B., Vadrevu, K. P., et al. (2013). Active fires from the Suomi NPP Visible Infrared Radiometer Suite: Product status and first evaluation results. *Journal of Geophysical Research*. http://dx.doi.org/10.1002/2013JD020453 (in press)..

Davies, D. K., Ilavajhala, S., Wong, M. M., & Justice, C. O. (2009). Fire information for resource management system: Archiving and distributing MODIS active fire data. *IEEE Transactions on Geoscience and Remote Sensing*, *47*(1), 72–79.

Elvidge, C. D., Kroehl, H. W., Kihn, E. A., Baugh, K. E., Davis, E. R., & Hao, W. M. (1996). *Algorithm for the retrieval of fire pixels from DMSP operational linescan system data.* Biomass burning and global change: Remote sensing, modeling and inventory development, and biomass burning in Africa, *1*. (pp. 73–85), 73–85.

Elvidge, C. D., Zhizhin, M., Hsu, F. -C, & Baugh, K. E. (2013). VIIRS nightfire: Satellite pyrometry at night. *Remote Sensing*, *5*, 4,423–4,449.

Flasse, S. P., & Ceccato, P. (1996). A contextual algorithm for AVHRR fire detection. *International Journal of Remote Sensing*, *17*(2), 419–424.

Giglio, L., Csiszar, I., Restas, Á., Morisette, J. T., Schroeder, W., Morton, D., et al. (2008). Active fire detection and characterization with the advanced spaceborne thermal emission and reflection radiometer (ASTER). *Remote Sensing of Environment*, *112*, 3055–3063.

Giglio, L., Descloitres, J., Justice, C. O., & Kaufman, Y. J. (2003). An enhanced contextual fire detection algorithm for MODIS. *Remote Sensing of Environment*, *87*, 273–282.

Giglio, L., Loboda, T., Roy, D. P., Quayle, B., & Justice, C. O. (2009). An active-fire based burned area mapping algorithm for the MODIS sensor. *Remote Sensing of Environment*, *113*(2), 408–420.

Hillger, D., Kopp, T., Lee, T., Lindsey, D., Seaman, C., Miller, S., et al. (2013). First-light imagery from Suomi NPP VIIRS. *Bulletin of the American Meteorological Society*. http://dx.doi.org/10.1175/BAMS-D-12-00097.1.

Ichoku, C., Giglio, L., Wooster, M. J., & Remer, L. A. (2008). Global characterization of biomass-burning patterns using satellite measurements of fire radiative energy. *Remote Sensing of Environment*, *112*, 2950–2962.

Joint Polar Satellite System (JPSS) (2013). Common data format control book – external (CDFCB-X) – volume III block 1.2.3 (effective date: July 2, 2013)– SDR/TDR formats, document number: 474-00001-03-B0123. http://npp.gsfc.science.sciencedocuments

Justice, C. O., Giglio, L., Korontzi, S., Owens, J., Morisette, J. T., Roy, D., et al. (2002). The MODIS fire products. *Remote Sensing of Environment*, *83*, 244–262.

Justice, C. O., Román, M.O., Csiszar, I., Vermote, E. F., Wolfe, R. E., Hook, S. J., et al. (2013). Land and cryosphere products from Suomi NPP VIIRS: Overview and status. *Journal of Geophysical Research, [Atmospheres], 118*. http://dx.doi.org/10.1002/jgrd.50771.

Kaufman, Y. J., Justice, C. O., Flynn, L. P., Kendall, J.D., Prins, E. M., Giglio, L., et al. (1998). Potential global fire monitoring from EOS-MODIS. *Journal of Geophysical Research*, *103*(D24), 32,215–32,238.

Morisette, J. T., Giglio, L., Csiszar, I., & Justice, C. O. (2005). Validation of the MODIS active fire over Southern Africa with ASTER data. *International Journal of Remote Sensing*, *26*(19), 4239–4264.

Roy, D., Boschetti, L., Justice, C. O., & Ju, J. (2008). The collection 5 MODIS burned area product—Global evaluation by comparison with the MODIS active fire product. *Remote Sensing of Environment*, *112*(9), 3690–3707.

Schroeder, W., Prins, E., Giglio, L., Csiszar, I., Schmidt, C., Morisette, J. T., et al. (2008). Validation of GOES and MODIS active fire detection products using ASTER and ETM + data. *Remote Sensing of Environment*, *112*, 2711–2726.

Smith, A. M. S., Tinkham, W. T., Roy, D. P., Boschetti, L., Kremens, R. L., Kumar, S. S., Sparks, A. M., & Falkowski, M. J. (2013). Quantification of fuel moisture effects on biomass consumed derived from fire radiative energy retrievals. *Geophysical Research Letters*, *40*. http://dx.doi.org/10.1002/2013GL058232.

Stroppiana, D., Pinnock, S., & Grégoire, J. -M. (2000). The Global Fire Product: Daily fire occurrence from April 1992 to December 1993 derived from NOAA AVHRR data. *International Journal of Remote Sensing*, *21*, 1279–1288.

Wolfe, R. E., Lin, G., Nishihama, M., Tewari, K. P., Tilton, J. C., & Isaacman, A.R. (2013). Suomi NPP VIIRS prelaunch and on-orbit geometric calibration and characterization. *Journal of Geophysical Research, [Atmospheres], 118*, 11,508–11,521. http://dx.doi.org/10.1002/jgrd.50873.